Supporting Information

Synergizing Interventional Photothermal Therapy and Immunotherapy with an Iron Oxide Nanoplatform for the Treatment of Pancreatic Cancer

Meng Wang[1], Yong Li[3], Miao Wang[2], Kaili Liu[4], Ashley R. Hoover[4], Min Li[5], Rheal A Towner[6], Priyabrata Mukherjee[7], Feifan Zhou[2]*, Junle Qu[1]*, and Wei R Chen[4]*

[1] Key Laboratory of Optoelectronic Devices and Systems of Ministry of Education and Guangdong Province, College of Physics and Optoelectronic Engineering, Shenzhen University, Shenzhen, 518060, China.

[2] School of Biomedical Engineering, Hainan University, Haikou, 570228, China.

[3] Interventional Therapy Department, Tianjin Key Laboratory of Cancer Prevention and Therapy, Tianjin Medical University Cancer Institute and Hospital, Tianjin, 300060, China.

[4] Stephenson School of Biomedical Engineering, University of Oklahoma, Norman, Oklahoma 73019, USA.

[5] Department of Medicine, Department of Surgery, University of Oklahoma Health Sciences Center, Oklahoma City, Oklahoma, USA.

[6] Advanced Magnetic Resonance Center, Oklahoma Medical Research Foundation, Oklahoma City, Oklahoma, USA.

[7] Department of Pathology, University of Oklahoma Health Sciences Center, Oklahoma City, Oklahoma, USA.

***Corresponding authors:**

Feifan Zhou: zhouff@hainanu.edu.cn

Junle Qu: jlqu@szu.edu.cn.

Wei R. Chen: Wei-R-Chen@ou.edu.

Supplementary Figures

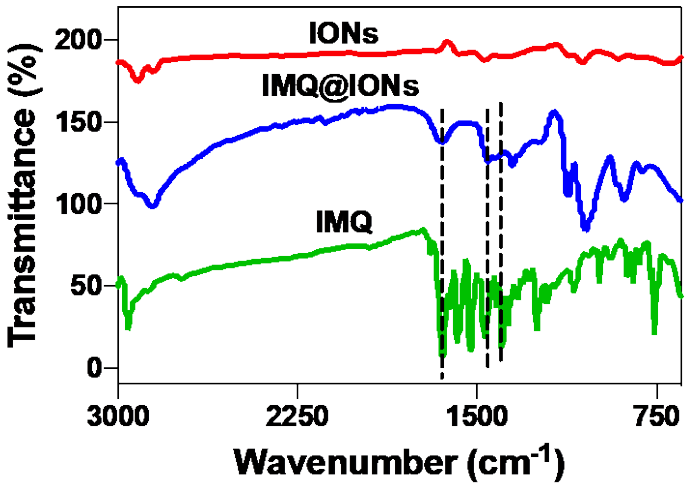

Fig. S1. Fourier transform infrared (FT-IR) spectra of IONs, IMQ@IONs, and IMQ.

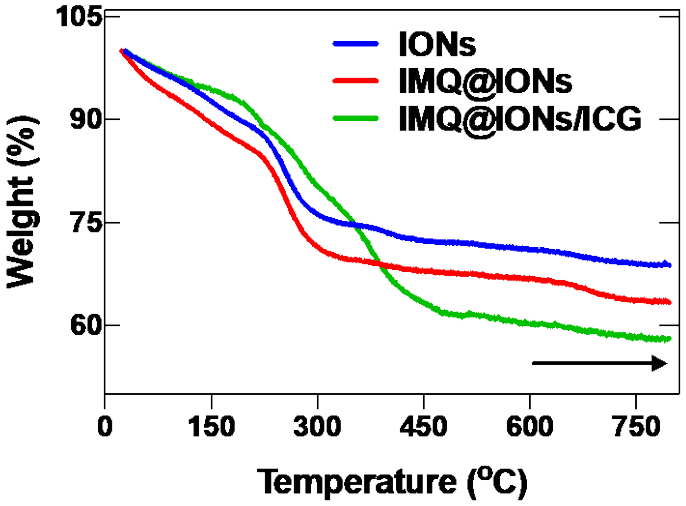

Fig. S2. Thermogravimetric analysis (TGA) of IONs, IMQ@IONs, and IMQ@IONs/ICG under N_2 atmosphere in the temperature range of 25 - 800 °C at a rate of 10 °C min^{-1}.

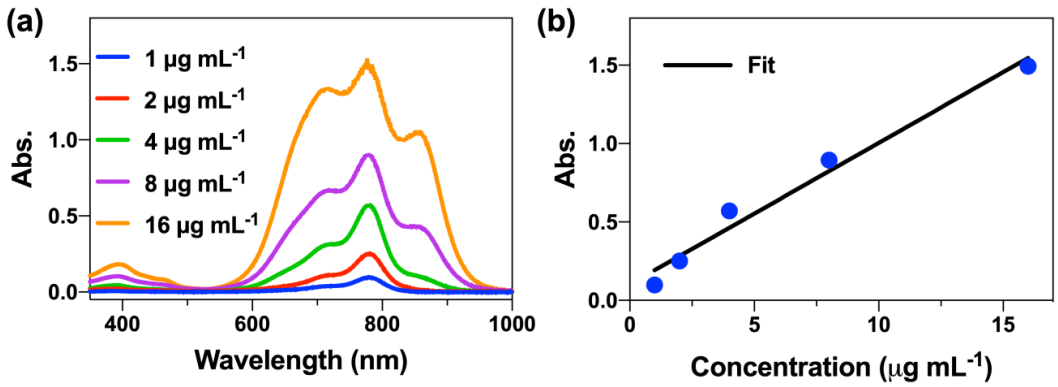

Fig. S3. Determination of ICG loading on IMQ@IONs/ICG by UV-vis spectra. (A) Absorption spectra of ICG solution at different concentrations. (B) The standard curve of ICG absorption at 790 nm, which was used for determination of the load rate of ICG.

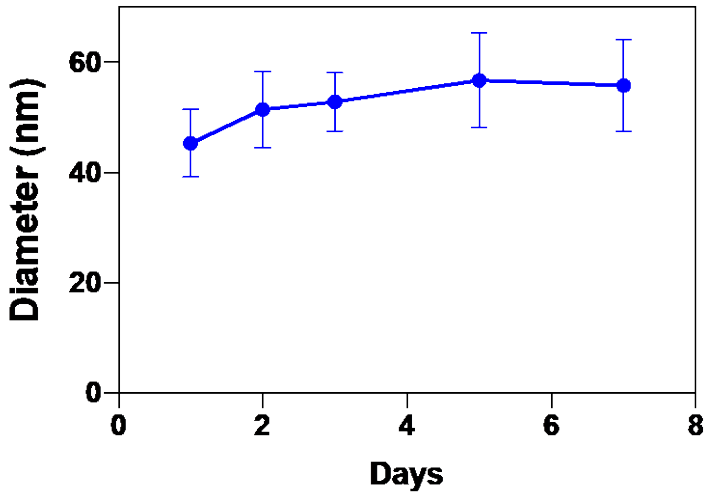

Fig. S4. Hydrodynamic diameter distribution of IMQ@IONs/ICG after being immersed in serum at different time point. Data are expressed as means ± SD (n = 3).

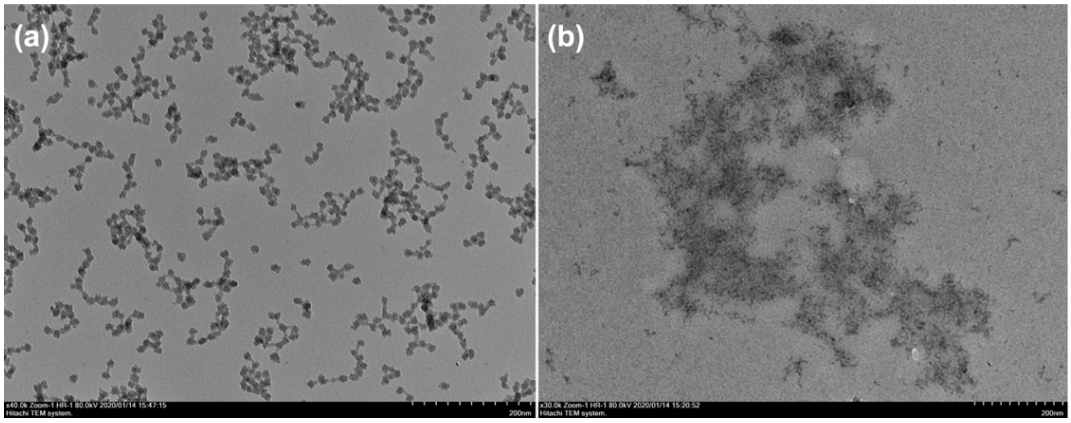

Fig. S5. Transmission electron microscope (TEM) images of IMQ@IONs/ICG after incubation in (A) pH 7.4 PBS and (B) pH 6.8 PBS for 2 h.

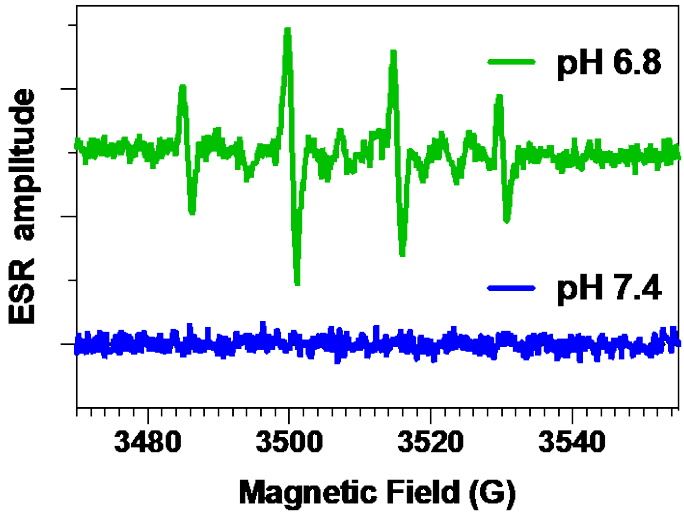

Fig. S6. Electron spin resonance (ESR) spectra of IMQ@IONs NPs in the presence of H_2O_2 at different pHs. 5-diethoxyphosphoryl-5-methyl-1-pyrroline N-oxide (DEPMPO) was used as the spin trap agent.

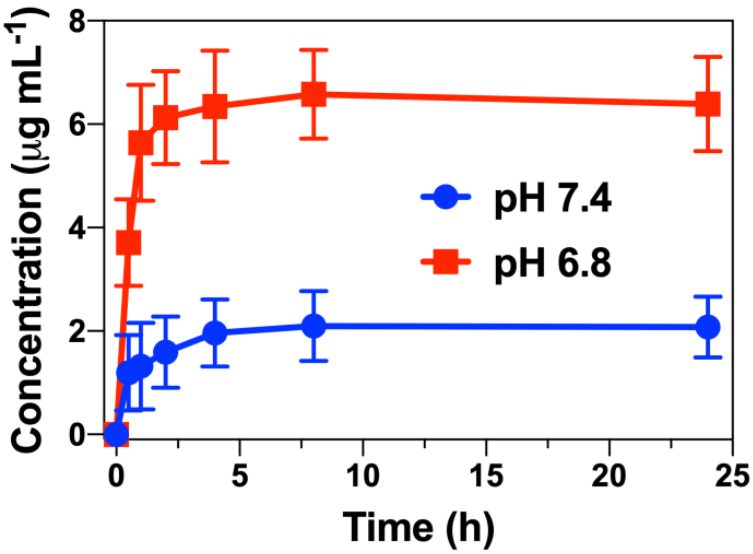

Fig. S7. Cumulative release of IMQ from IMQ@IONs nanoparticles in pH 7.4 PBS buffer and pH 6.8 PBS buffer at room temperature. Data are expressed as means ± SD (n = 3).

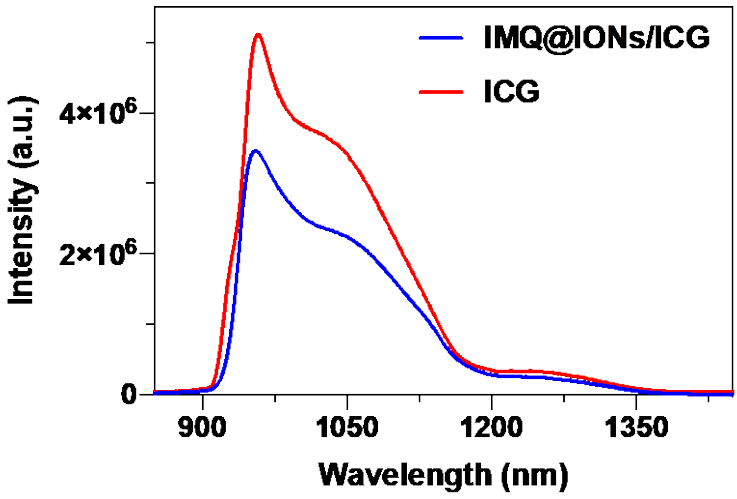

Fig. S8. Fluorescence spectra of IMQ@IONs/ICG and ICG under an 805-nm laser excitation.

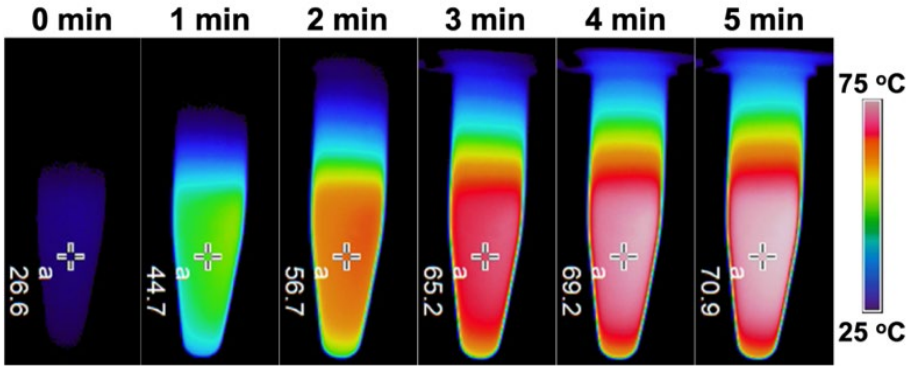

Fig. S9. Infrared (IR) thermal images of IMQ@IONs/ICG solution under laser irradiation (805 nm, 0.75 W cm^{-2} for 5 min).

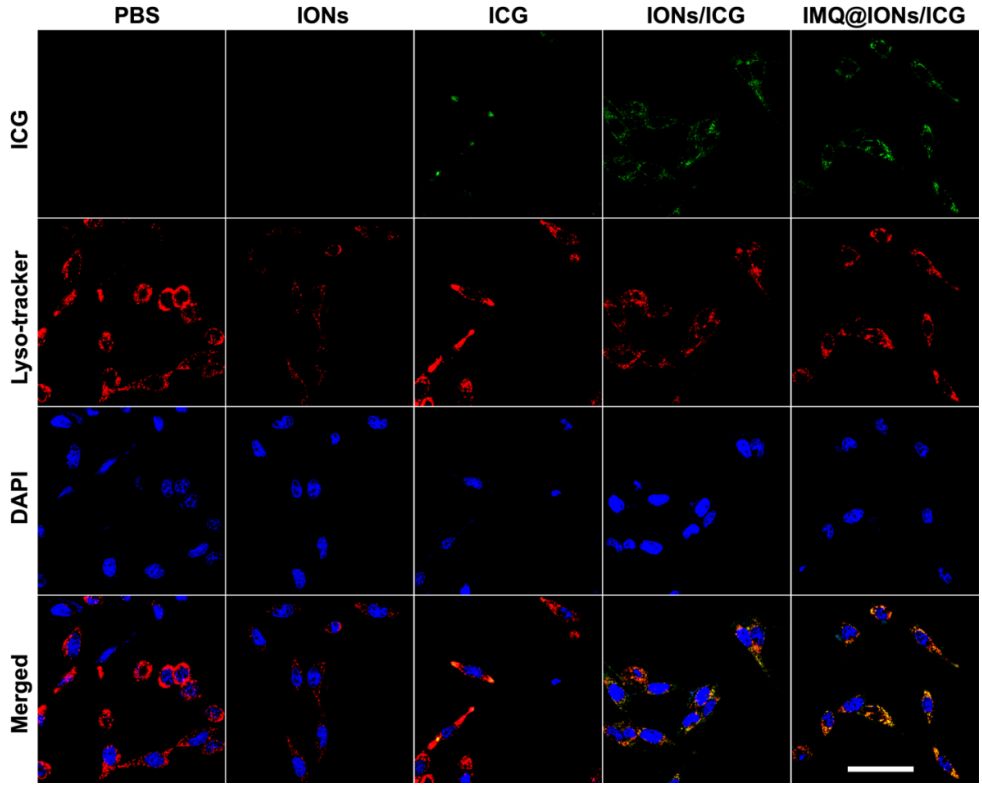

Fig. S10. Representative fluorescence images of Panc02-H7 cells after 2 h incubation with IONs (100 μg mL^{-1}), ICG (15 μg mL^{-1}), IONs/ICG (100 μg mL^{-1}), and IMQ@IONs/ICG (100 μg mL^{-1}). Green: ICG, Red: Lyso-tracker, Blue: DAPI. (Scale bar = 50 μm).

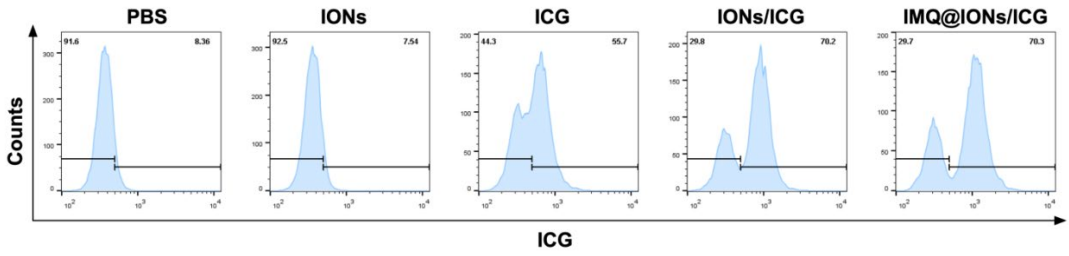

Fig. S11. Cellular uptake of ICG by Panc02-H7 cells incubation with PBS, IONs (100 μg mL^{-1}), ICG (15 μg mL^{-1}), IONs/ICG (100 μg mL^{-1}), and IMQ@IONs/ICG (100 μg mL^{-1}), analyzed by flow cytometry.

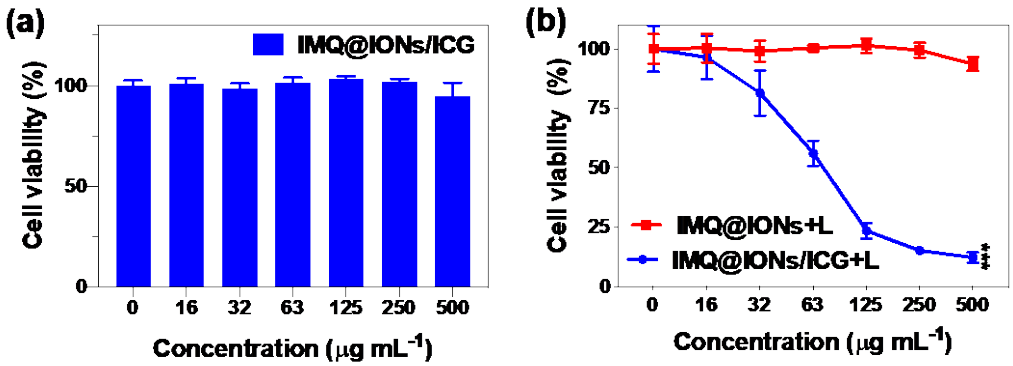

Fig. S12. Cytotoxicity of nanoparticles on Panc02-H7 cells with or without laser irradiation. (A) *In vitro* cytotoxicity of IMQ@IONs/ICG on Panc02-H7 cells after incubation for 24 h, analyzed by a CCK-8 assay. (B) *In vitro* phototoxicity of IONs/ICG and IMQ@IONs/ICG on Panc02-H7 cells analyzed by a CCK-8 assay (Laser: 805 nm, 0.75 W cm^{-2} for 5 min, ***$p < 0.001$ vs IMQ@IONs). Data are expressed as means ± SD (n = 4).

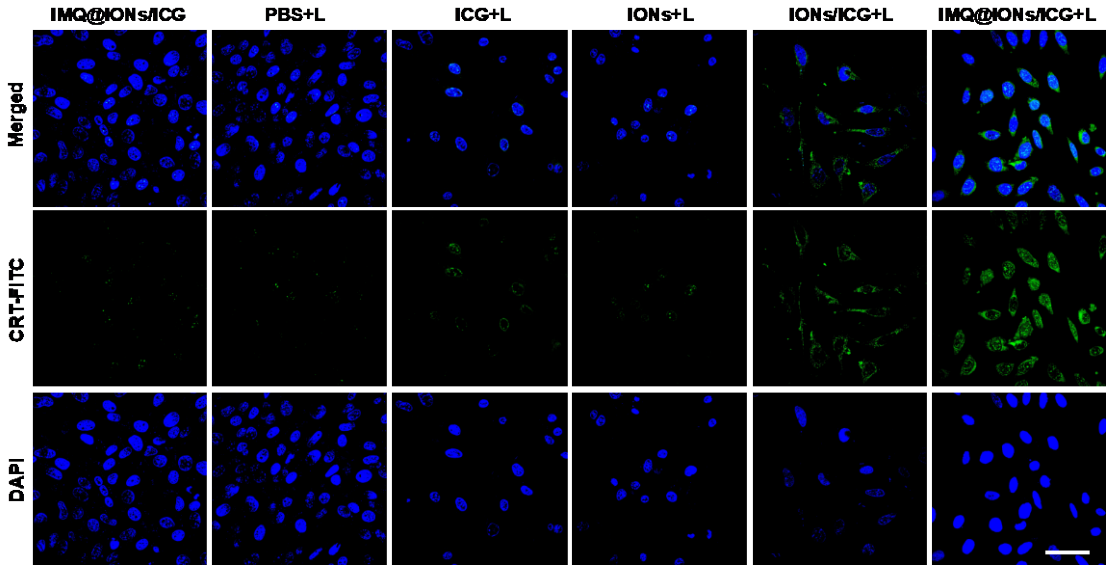

Fig. S13. Representative fluorescence images of Panc02-H7 cells showing calreticulin (CRT) exposure on the surface after the treatment with IMQ@IONs/ICG, PBS + L, ICG+L, IONs + L, IONs/ICG + L, or IMQ@IONs/ICG + L. Green: CRT-FITC, Blue: DAPI. (Laser: 805 nm, 0.75 W cm^{-2} for 5 min, Scare bar = 50 μm.)

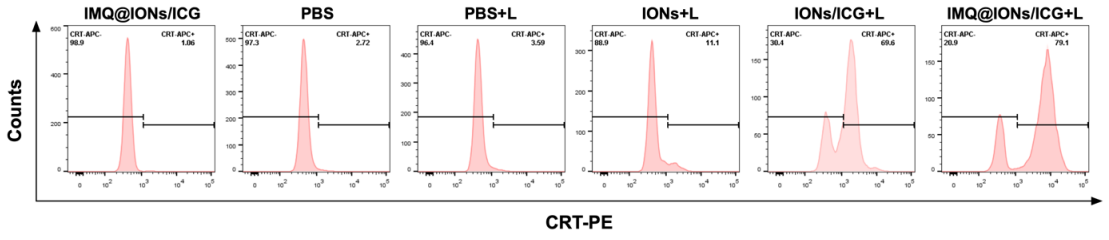

Fig. S14. Flow cytometry analysis of CRT exposure on the surface of Panc02-H7 cells after the treatment with IMQ@IONs/ICG, PBS, PBS + L, IONs + L, IONs/ICG + L, or IMQ@IONs/ICG + L.

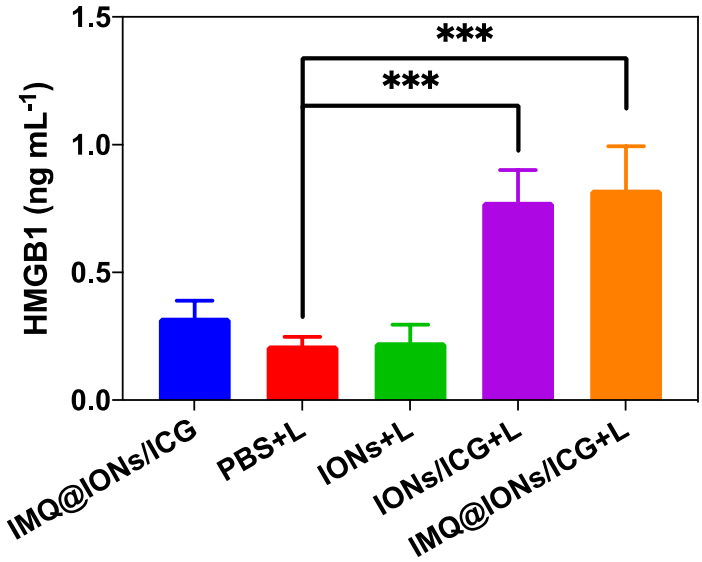

Fig. S15. The release of high mobility group 1 (HMGB1) from Panc02-H7 cells after the treatment with PBS + L, IONs + L, IONs/ICG + L, or IMQ@IONs/ICG + L (Laser: 805 nm, 0.75 W cm^{-2} for 5 min; ***p < 0.001 vs PBS + L, one-way ANOVA with Tukey test). Data are expressed as means ± SD (n = 4).

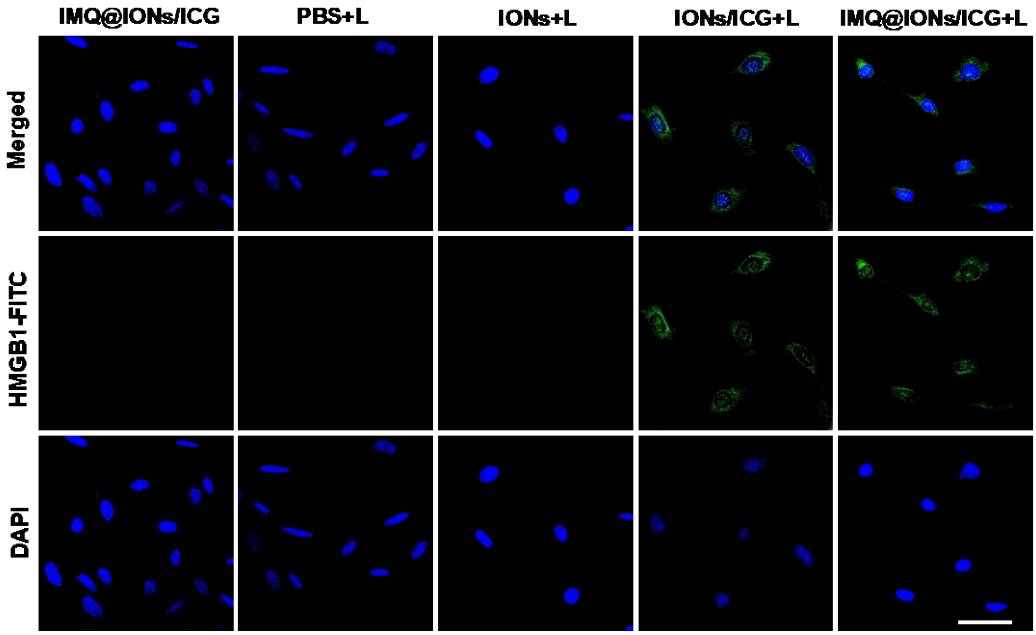

Fig. S16. Representative fluorescence images of Panc02-H7 cells showing HMGB1 exposure after the treatment with IMQ@IONs/ICG, PBS + L, IONs + L, IONs/ICG + L, or IMQ@IONs/ICG + L. Green: HMGB1-FITC, Blue: DAPI. (Laser: 805 nm, 0.75 W cm^{-2} for 5 min, Scare bar = 50 μm.)

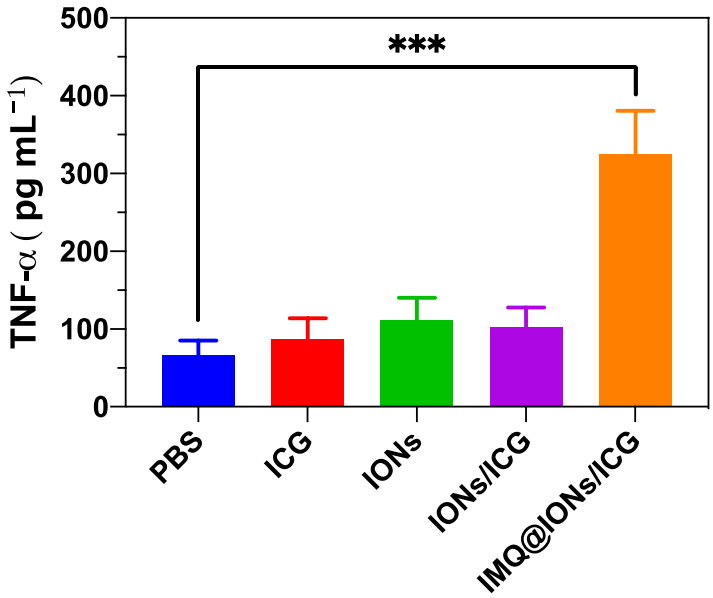

Fig. S17. Secretion of TNF-α from BMDCs stimulated by indicated nanoparticles (***$p < 0.001$ vs PBS, one-way ANOVA with Tukey test). Data are expressed as means ± SD (n = 4).

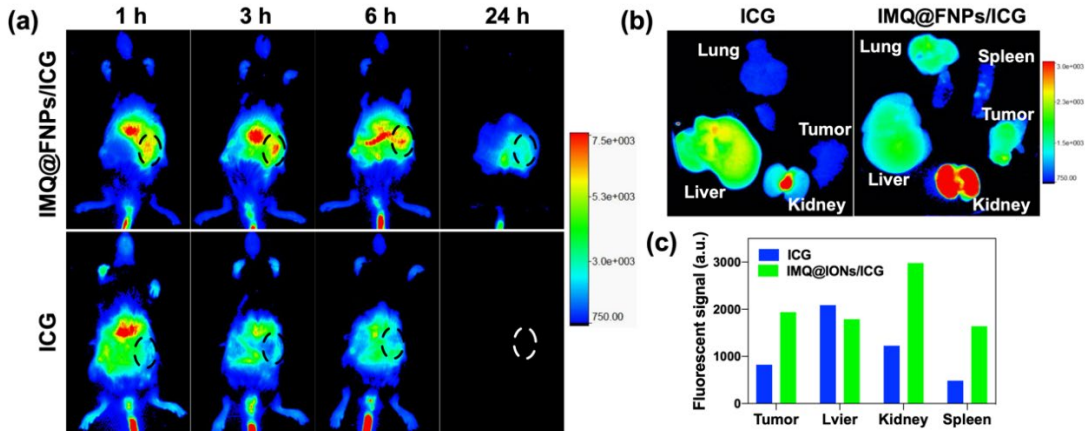

Fig. S18. Tissue distribution of IMQ@IONs/ICG analyzed by *in vivo* fluorescence imaging. (A) Representative fluorescence images of Panc02-H7 tumor-bearing mice at indicated time points (1, 3, 6, and 24 h) after intravenous injection of ICG (40 μg mL^{-1}, 100 μL) and IMQ@IONs/ICG (10 mg mL^{-1}, 100 μL). Tumors are circled with black dashed lines. (B) Ex vivo fluorescence images of excised organs and tumors at 6 h post injection of ICG and IMQ@IONs/ICG. (C) The semi-quantitative analysis of fluorescence signals captured from these organs and tumors 6 h post injection.

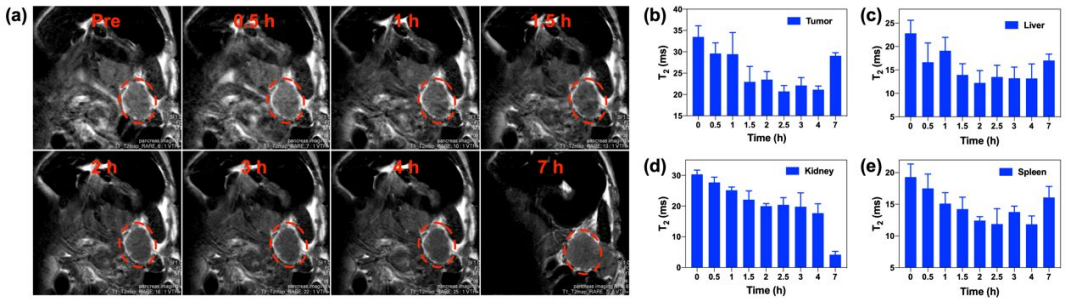

Fig. S19. Tissue distribution of IMQ@IONs/ICG analyzed by MRI. (A) Representative T_2-weighted MR images of Panc02-H7 tumor-bearing mice at indicated time points after intravenous injection of IMQ@IONs/ICG (10 mg mL^{-1}, 100 μL). Tumors are circled with red dashed lines. Corresponding representative T_1-weighted signals of (B) tumor, (C) liver, (D) kidney, and (E) spleen at different time points after intravenous injection of IMQ@IONs/ICG.

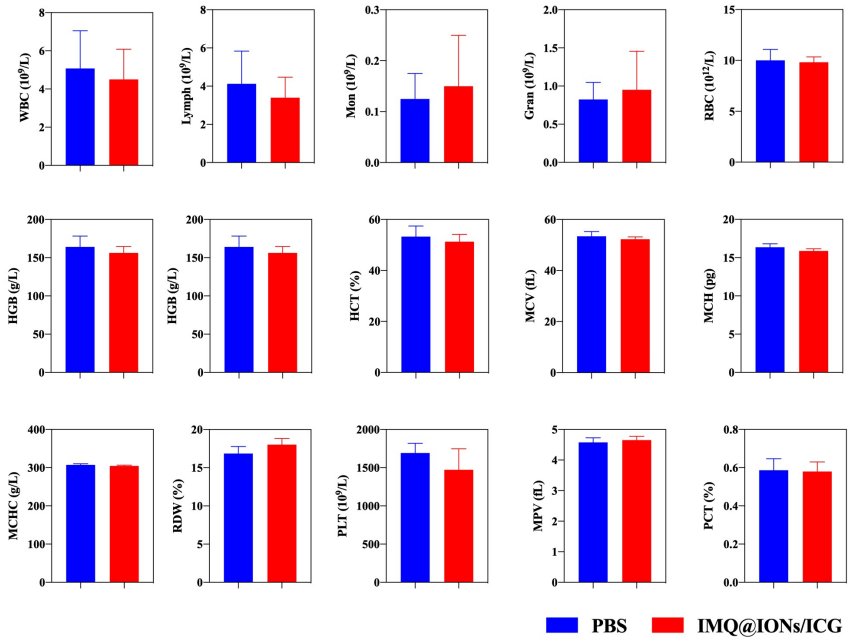

Fig. S20. Hematology and blood biochemistry analysis of mice *i.v.* injected with IMQ@IONs/ICG (100 mg/kg) at 15th day. The examined parameters included: white blood cell count (WBC), lymphocyte count (Lymph), monocytes count (Mons), neutrophilic granulocyte count (Gran), red blood cell count (RBC), hemoglobin (HGB), hematocrit (HCT), mean corpuscular volume (MCV), mean corpuscular hemoglobin (MCH), mean corpuscular hemoglobin concentration (MCHC), red cell volume distribution width (RDW), platelet (PLT), mean platelet volume (MPV), platelet distribution width (PDW), thrombocytocrit (PCT). Data are expressed as means ± SD (n = 4).

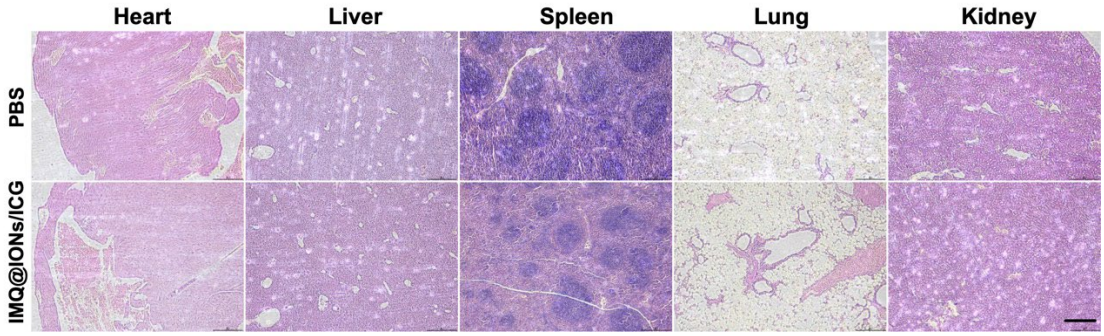

Fig. S21. Representative H&E-stained images of major organs from the healthy mice after intravenous injection of PBS (100 μL) or IMQ@IONs/ICG (10 mg mL^{-1}, 100 μL). The scare bar = 200 μm.

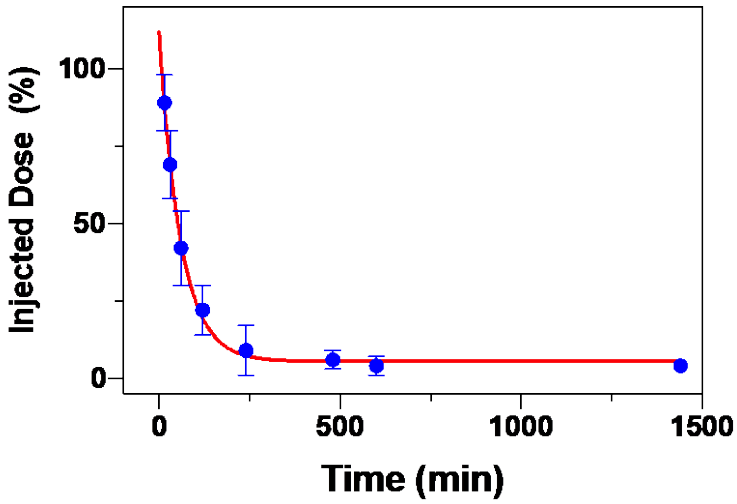

Fig. S22. Pharmacokinetics of IMQ@FNPs/ICG. C57BL6 mice were *i.v.* injected with IMQ@FNPs/ICG to study the blood circulation time of IMQ@FNPs/ICG. Blood samples were collected and measured by ICP-OES at various time points post injection (up to 24 hours). The half-life of the IMQ@FNPs/ICG blood circulation was estimated to be ~ 41.2 mins. Data are expressed as means ± SD (n = 4).

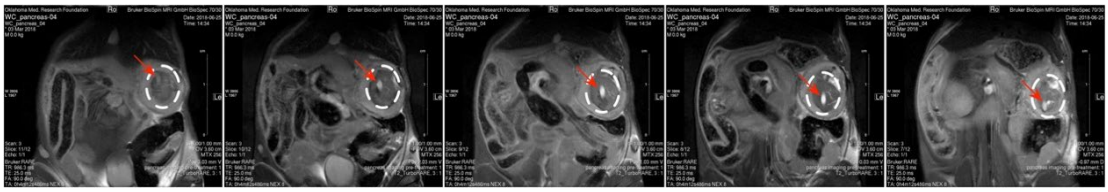

Fig. S23. Representative T_2-weighted MR images of mice showing the location of optical fiber in pancreatic tumor during interventional photoimmunotherapy. Tumors are circled with white dashed lines, and red arrows point to the optical fiber.

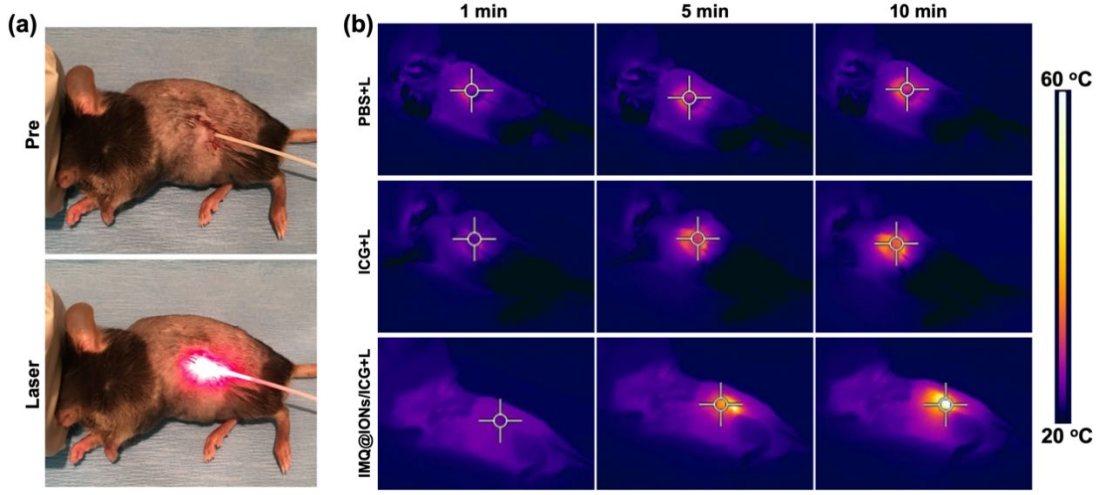

Fig. S24. IR thermal imaging during IPTT. (A) Representative photo images of Panc02-H7 tumor-bearing mice treated with interventional photoimmunotherapy. (B) Representative IR thermal images of Panc02-H7 tumor-bearing mice treated with PBS, ICG, and IMQ@IONs/ICG under an 805-nm laser irradiation (1 W for 10 min).

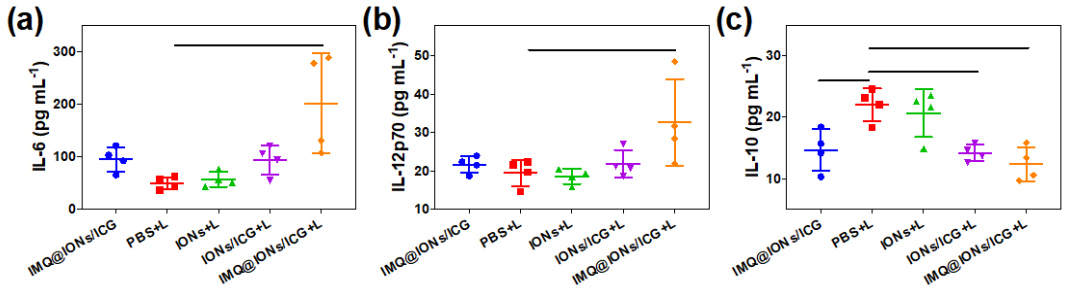

Fig. S25. Systemic immune response analysis after different treatments. Cytokine levels of (A) IL-6, (B) IL-12, and (C) IL-10 in sera from mice isolated at 7 days post different treatments (*p < 0.05 vs PBS, **p < 0.01 vs PBS, ***p < 0.001 vs PBS, one-way ANOVA with Tukey test). Data are expressed as means ± SD (n = 4).

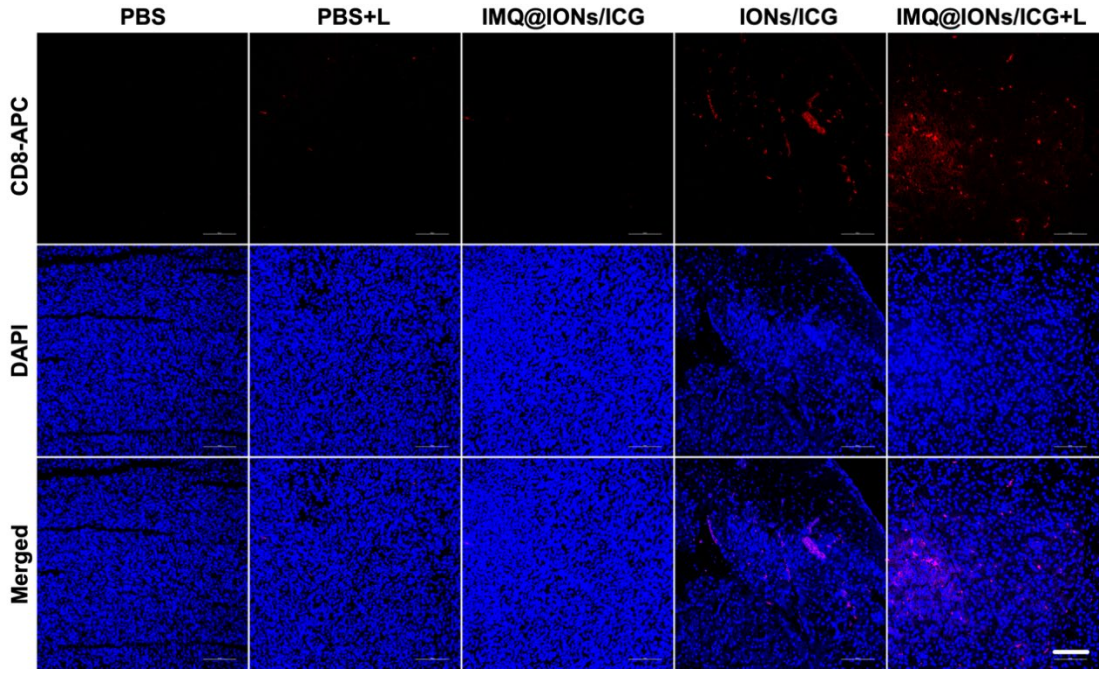

Fig. S26. Representative images of tumor section staining of $CD8^+$ T cells (Red) and DAPI (Blue) 7 days after different treatments. Scale bar = 100 μm.

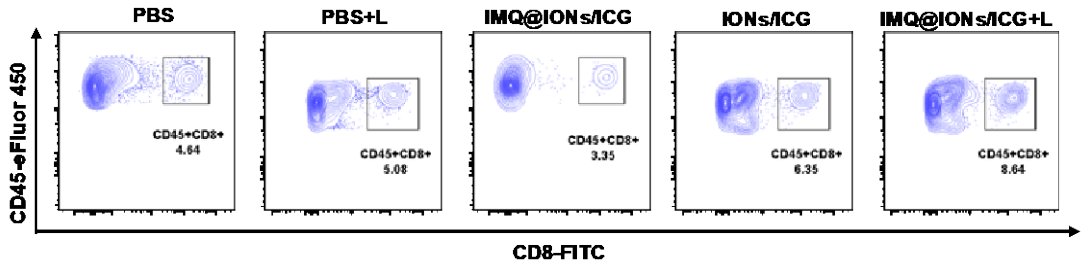

Fig. S27. Representative flow plots used to quantify changes in the relative abundance of $CD8^+$ cell subpopulations in tumors following different treatments.

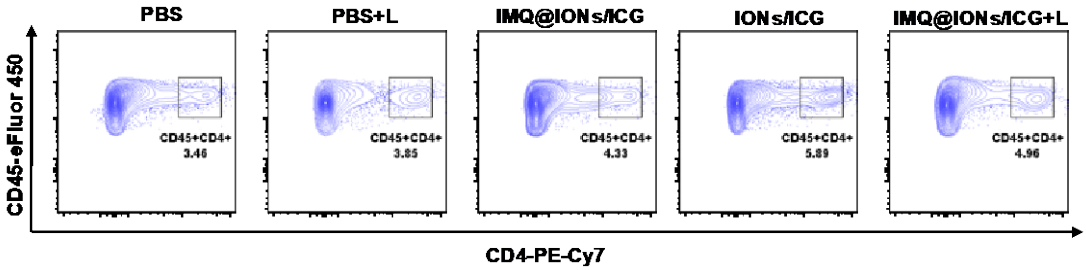

Fig. S28. Representative flow plots used to quantify changes in the relative abundance of $CD4^+$ cell subpopulations in tumors following different treatments.

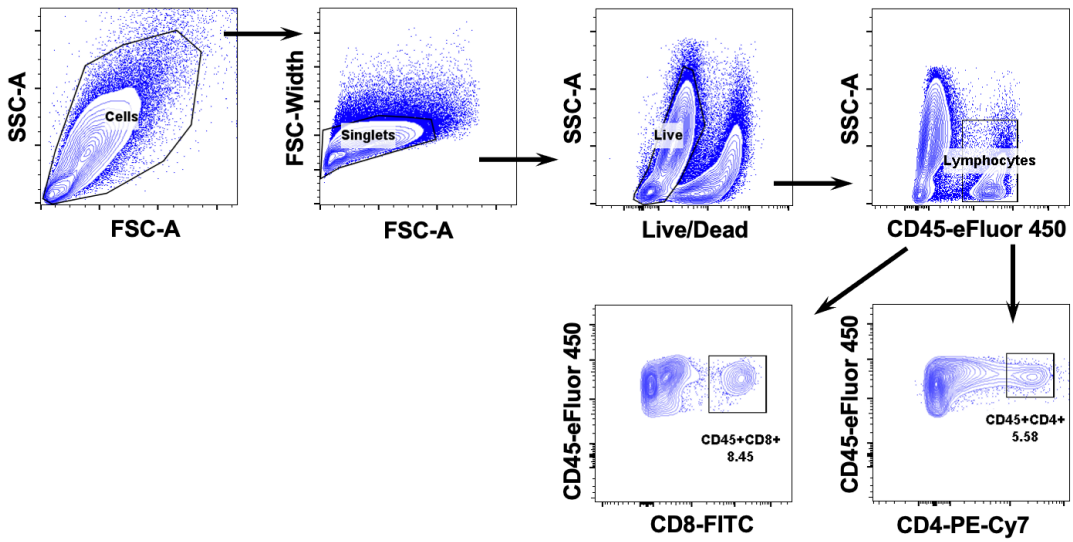

Fig. S29. Gating strategy determine frequencies of T cells from tumors. The gating strategy was performed based on exclusion of doublets by FSC-A and FSC-Width, exclusion of dead cells, selection of $CD45^+$, and further staining using CD8 and CD4 with appropriate fluorescent dyes to select $CD8^+$ or $CD4^+$ T cells, respectively.

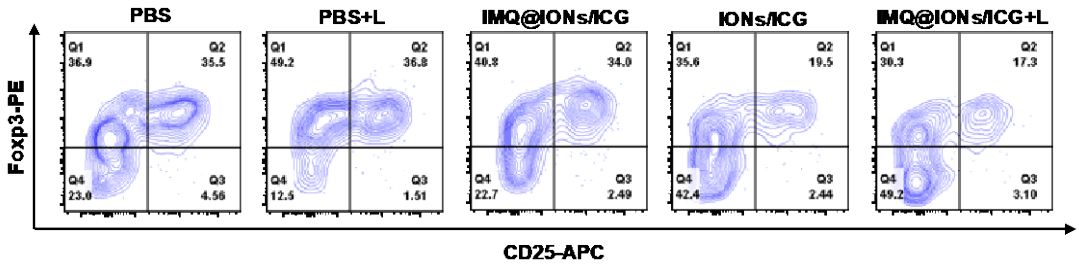

Fig. S30. Representative flow plots used to quantify changes in the relative abundance of T_{reg} subpopulations in tumors following different treatments.

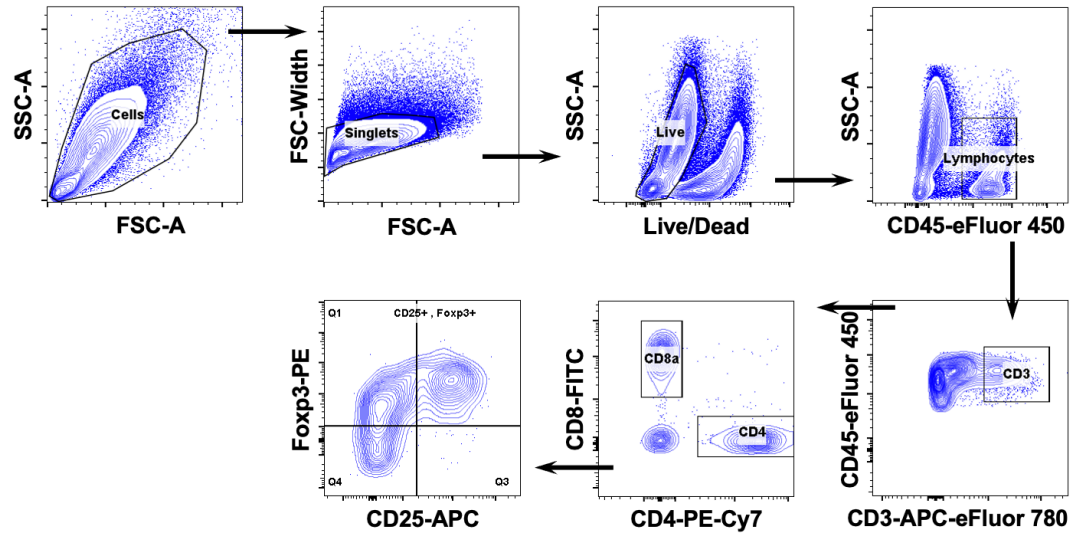

Fig. S31. Gating strategy determine frequencies of T_{regs} from tumors. The gating strategy was performed based on exclusion of doublets by FSC-A and FSC-Width, exclusion of dead cells, selection of $CD45^+$, selection of $CD3^+$, selection of $CD4^+$, and further staining using Foxp3 and CD25 with appropriate fluorescent dyes to select T_{regs}.

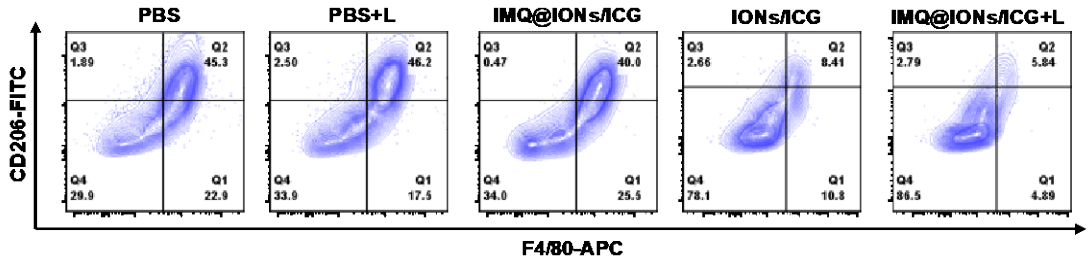

Fig. S32. Representative flow plots used to quantify changes in the relative abundance of M2-like TAM subpopulations in tumors following different treatments.

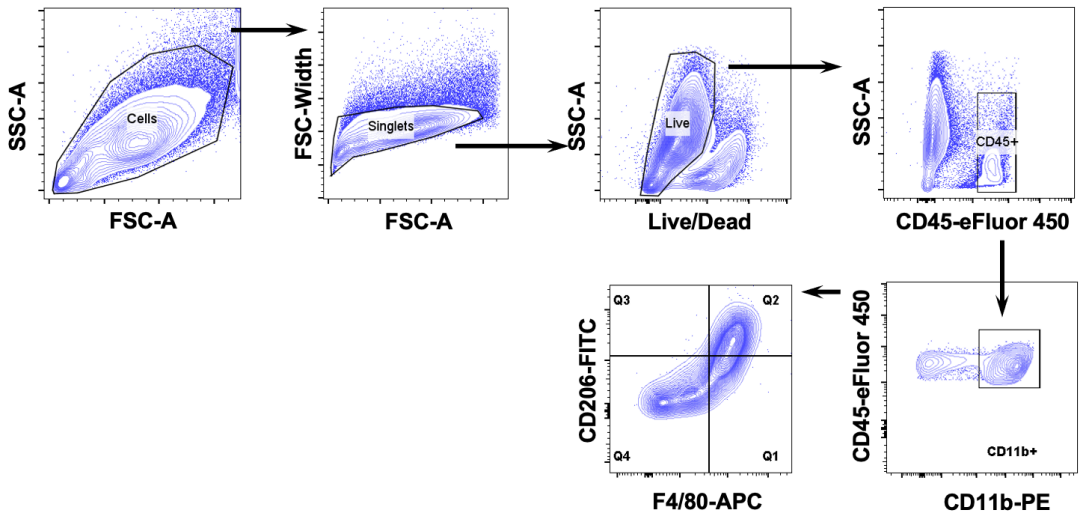

Fig. S33. Gating strategy determine frequencies of M2-like TAM from tumors. The gating strategy was performed based on exclusion of doublets by FSC-A and FSC-Width a), exclusion of dead cells, selection of $CD45^{+}$, selection of $CD11b^{+}$, and further staining using F4/80 and CD206 with appropriate fluorescent dyes to select M2-like TAM cells.

Experimental Section

Materials

$Fe(CO)_5$, cetyltrimethylammonium bromide (CTAB, >99%), indocyanine green (ICG, >90%), imiquimod (IMQ), H_2O_2 (30%), methanol, ethanol, 1-hexanol, n-dodecane, and diethylene glycol (DEG) were purchased from Sigma-Aldrich (St Louis, MO). DSPE-PEG (1,2-distearoyl-sn-glycero-3-phosphoethanolamine-N[methoxy(polyethylene glycol)]) with the PEG molecular weight 2000 (DSPE-PEG_{2k}) was obtained from Avanti Polar Lipids (Alabaster, AL). Dulbecco's modified Eagle's medium (DMEM), Roswell Park Memorial Institute (RPMI) 1640 medium, fetal bovine serum (FBS), 0.25% trypsin-EDTA, penicillin, and streptomycin were purchased from Gibco (Grand Island, NY).

Cell Line

Panc02-H7, an aggressive pancreatic cell line, was derived from Panc02 that was established by implanting 3-methylcholanthrene into the pancreas of a C57BL/6 mouse. Panc02-H7 cells were tested and verified to be free of Mycoplasma and used after two passages from thawing. The cells were cultured with DMEM, supplemented with 10% FBS, penicillin (100 U mL^{-1}), and streptomycin (100 mg mL^{-1}), in a humidified incubator with 5% CO_2, 95% air at 37 °C (NuAire).

Characterization of Nanoparticles

TEM images were obtained via JEOL-2010 TEM (JEOL, Japan). The amounts of loaded ICG and IMQ were quantitatively evaluated via UV–vis–NIR spectrophotometer (Cary 50 Bio, USA). The loading capacity of ICG was calculated

using the following equation: loading capacity of ICG (%) = (weight of ICG - weight of unloaded ICG) / (weight of IMQ@IONs/ICG) × 100%. The loading capacity of IMQ was calculated using the following equation: loading capacity of IMQ (%) = (weight of loaded IMQ) / (weight of IMQ@IONs/ICG) × 100%. Fourier transform infrared (FTIR) spectra were recorded in KBr discs on a Magna 750 FTIR spectrometer. The hydrodynamic diameter distribution of nanoparticles was determined by means of dynamic light scattering (DLS) measurement (Nano ZS ZEN3600, Malvern).

Thermal Stability of IMQ@IONs/ICG

IMQ@IONs/ICG aqueous solution (0.5 mg mL^{-1} in 0.3 mL) was irradiated with an 805 nm laser at 0.75 W cm^{-2} for 5 min, and then naturally cooled to room temperature. The above process was repeated three times.

Calculation of the photothermal conversion efficiency of IMQ@IONs/ICG

The photothermal conversion efficiency of IMQ@IONs/ICG was determined according to a previously reported method as follows Equation [1].

$$\eta = \frac{hA\Delta T - Q_s}{I(1 - 10^{-A_\lambda})}$$

Where h is the coefficient of heat transfer, $\boldsymbol{A}$ is the container surface area, $\boldsymbol{\Delta T}$ is the temperature change of the IMQ@IONs/ICG solution, $\boldsymbol{I}$ is the power density of the 805 nm laser, $\boldsymbol{A_\lambda}$ is the absorbance of the solution of IMQ@IONs/ICG at 805 nm, and $\boldsymbol{Q_s}$ is the heat associated with the light absorbance of the water.

Cytotoxicity and Apoptosis Assay

For cell viability analysis, Panc02-H7 cells were seeded into 96-well plates at a density of 1×10^3 cells per well and cultured for 12 h. The cells were treated with ICG, IONs, and IMQ@IONs/ICG at various concentrations. After incubation for 2 h, the cells were irradiated with or without an 805 nm laser (0.75 W cm^{-2} for 5 min). The cells were further incubated for 24 h and cell viability was detected via CCK-8 assay, according to the manufacturer's protocol. In addition, treated Panc02-H7 cells were stained with Calcein AM and PI and observed with confocal microscopy, to verify the cell death.

Apoptosis of tumor cells was assessed by Annexin V-FITC/PI Cell Apoptosis Kit. Cells were seeded into 12-well plates (5×10^5 cells/well) and cultured for 12 h. Cells were treated with PBS, ICG, IONs, and IMQ@IONs/ICG at an equivalent ICG concentration (30 μg mL^{-1}). After 2 h of incubation, the cells were irradiated with an 805 nm laser (0.75 W cm^{-2} for 5 min), followed by a further 24 h incubation. IMQ@IONs/ICG without laser irradiation served as the dark control. The cell apoptosis was detected by flow cytometry with Annexin V-FITC/PI staining, according to the manufacturer's protocol.

Detection of ICD Biomarkers

Surface-exposure of CRT on Panc02-H7 cells was assessed *via* flow cytometry and immunofluorescence. Cells were seeded into 8-well chambered slides and cultured for 12 h. The cells were incubated with PBS, IONs, or IMQ@IONs/ICG for 2 h and irradiated with an 805 nm laser (0.75 W cm^{-2} for 5 min). Cells treated with IMQ@IONs/ICG without laser irradiation served as dark control. After a further 24 h

of incubation, cells were washed twice with PBS and then incubated with anti-calreticulin antibody for 2 h at 4 °C. Subsequently, the cells were washed twice with PBS and incubated with PE-conjugated secondary antibody (BioLegend, USA) for 1 h. The samples were analyzed by flow cytometer to identify cell surface CRT. For immunofluorescence analysis, the treated cells were further stained with DAPI, and observed *via* fluorescence microscopy (Olympus, Japan). Extracellular HMGB1 in conditioned media (serum-free) secreted from treated cells were measured *via* HMGB1 ELISA Kit (R&D systems), following the manufacturer's instructions.

In Vitro Dendritic Cell Stimulation

Bone marrow–derived dendritic cells (BMDCs) were generated from 8 weeks old C57BL/6 female mice, according to an established method [2]. For *in vitro* DC stimulation experiments, ICG, IONs or IMQ@IONs/ICG were incubated with 10^6 BMDCs for 24 h. After various treatments, BMDCs stained with anti-CD86-PE and anti-CD80-FITC antibody were analyzed via Stratedigm S1200Ex flow cytometer (Stratedigm, USA).

Multimodal Imaging

Tumor bearing mice were randomly divided into two groups. About 7-10 days after tumor inoculation, when the pancreatic tumors reached a size of 8 mm (approximately 300 mm^3) in diameter, mice were injected with ICG or IMQ@IONs/ICG by *i.v*. The FL signals of ICG were recorded with an IVIS spectrum imaging system (Xenogen, USA) (ex: 780 nm) at 1, 4, and 24 h. The FL images of mice before injection served as blank control. For the biodistribution study, mice were

sacrificed 24 h post injection, and both tumors and normal tissues were harvested and imaged. Similarly, MR images of the tumor sites were recorded with a 7.1 Tesla MR scanner (Bruker Biospin, USA) at pre, 0.5, 1, 1.5, 2, 3, 4 and 7 h. The MR images of mice before injection served as blank control.

MR temperature imaging and PRF-shift calculation

The temperature shift during interventional photothermal therapy was assessed using proton resonance frequency (PRF)-shift thermometry. Since the PRF-shift method had better temperature sensitivity, excellent linearity and near-independence with tissue type, it was the preferred choice for temperature MRI mapping. According to the Larmor equation, the phase obtained within a voxel at a temperature T was given as follows:

$$\varphi(T) = \gamma TE\left[\left(1 - \sigma_{tot}(T)\right)B_0 + \delta B_0\right]$$

Among them, φ(T) was the phase at a temperature T, γ was the gyromagnetic ratio of hydrogen ($\gamma/2\pi$ = 42.577 × 106 s^{-1} T^{-1}), TE was the echo time, σ_{tot}(T) was the total screening constant of the proton, B_0 was the main magnetic field of the MRI scanner and δB_0 was the local deviations from B_0.

When the temperature changed from T to T', the phase difference (Δφ) was measured in a voxel.

$$\Delta\varphi = \varphi(T') - \varphi(T) = \gamma TE\left(\sigma_{tot}(T) - \sigma_{tot}(T')\right)B_0 = -\gamma TE\alpha\Delta T B_0$$

Here, ΔT was the temperature difference between T' and T, and α was a proportionality constant in the linear temperature dependence of σ_{tot}.

The tumor-bearing mice were imaged under an external magnetic field of B_0 = 7.0

T and with an echo time of TE = 4 ms. The phase shift between successive images was calculated using the formula given in equation:

$$\Delta\varphi = \varphi_n - \varphi_0 = arctan\left(\frac{\Re(T_0)\Im(T_n) - \Re(T_n)\Im(T_0)}{\Re(T_0)\Re(T_n) + \Im(T_0)\Im(T_n)}\right)$$

where $\Re(T_n)$ refers to the real part of the nth image, $\Im(T_n)$ refers to the imaginary part of the nth image, and T_0 refers to the image captured at the start of laser treatment.

Then, the temperature shift can be calculated according to equation:

$$\Delta T = \frac{\Delta\varphi}{\alpha\gamma TEB_0}$$

Phase-drift correction and post-processing

Phase-drift was calculated for each 2D tomogram by finding the best fit first-order polynomial to the region of the data outside of the heating area. To determine the appropriate region of interest, a mask was generated by maximizing the contrast about the point 0.2 in magnitude which was qualitatively determined from histograms of the data to primarily exclude points in the MRI image outside of the animal tissue. The opening of the region of interest by a disc structural element with a radius of 5 pixels was then calculated to remove clean up the edges of the mask. The internal heating region of interest was determined by the union of the external region of interest with a mask generated from maximizing the contrast about the point -0.2 radians phase-shift which was qualitatively determined to denote the heating region. The internal region of interest was then opened with a disc structural element with a radius of 10 pixels and then dilated with a disc structural element with a radius of 5 pixels. The dilated internal region of interest was then clipped to the external region of interest and then subtracted

out from the external region of interest.

The phase-drift $\Delta\varphi_d$ can be thought of as the phase-shift within the external region of interest. As such, the phase shift within the external region of interest was fit to a first-order polynomial $\Delta\varphi_d = a_0 + a_x X + a_y Y$ where a_0 is the zeroth-order coefficient and a_x and a_y are the first-order coefficients along the X and Y dimensions, respectively. The phase-drift was then subtracted out from the phase-shift data, and the internal region of interest was re-calculated as above to serve as a mask for the temperature data.

Immunofluorescence Assay

Tumors were collected and frozen tissue sections of 6 μm thickness were prepared via cryostat. These sections were air-dried for at least 1 h and then fixed in acetone for 10 min at room temperature. After blocking with 20% donkey serum, the sections were incubated with antibodies, washed twice with PBS, and observed via fluorescence microscopy (Olympus, Japan).

References

[1] B. Li, Q. Wang, R. Zou, X. Liu, K. Xu, W. Li, J. Hu, Cu7.2S4 nanocrystals: a novel photothermal agent with a 56.7% photothermal conversion efficiency for photothermal therapy of cancer cells, Nanoscale 6(6) (2014) 3274-3282.

[2] J. Helft, J. Böttcher, P. Chakravarty, S. Zelenay, J. Huotari, Barbara U. Schraml, D. Goubau, C. Reis e Sousa, GM-CSF Mouse Bone Marrow Cultures Comprise a Heterogeneous Population of CD11c+MHCII+ Macrophages and Dendritic Cells,

Immunity 42(6) (2015) 1197-1211.